

Iron Opacity and the Pulsar of Supernova 1987A

Chris L. Fryer

Lick Observatory, University of California Observatories,
Santa Cruz, CA 95064
cfryer@ucolick.org

Stirling A. Colgate

Los Alamos National Laboratory,
MS B275, Los Alamos, NM 87545
colgate@lanl.gov

and

Philip A. Pinto

Steward Observatory, University of Arizona,
Tucson, AZ 85721
pinto@as.arizona.edu

ABSTRACT

Neutron stars formed in Type II supernovae are likely to be initially obscured by late-time fallback. Although much of the late-time fallback is quickly accreted via neutrino cooling, some material remains on the neutron star, forming an atmosphere which slowly accretes through photon emission. In this paper, we derive structure equations of the fallback atmosphere and present results of one-dimensional simulations of that fallback. The atmosphere remaining after neutrino cooling (L_ν) becomes unimportant ($L_\nu \lesssim L_{\text{Edd},e^-}$, the Compton Eddington limit) is only a fraction of the total mass accreted ($\lesssim 10^{-8} M_{\text{acc}} = 10^{-9} M_\odot$). Recombined iron dominates the opacity in the outer regions leading to an opacity $10^3 - 10^4$ times higher than that of electron scattering alone. The resultant photon emission of the remnant atmosphere is limited to $\lesssim 10^{-3} L_{\text{Edd},e^-}$. The late-time evolution of this system leads to the formation of a photon-driven wind from the accretion of the inner portion of the atmosphere, leaving, for most cases, a bare neutron star on timescales shorter than a year. The degenerate remnant of 1987a may not be a black hole. Instead, the fallback material may have already accreted or blown off in the accretion-driven wind. If the neutron star has either a low magnetic field or a low rotational spin frequency, we would not expect to see the neutron star remnant of 1987a.

Subject headings: stars: neutron – pulsars: general – supernovae: general

1. Introduction

The mechanism for Type II supernovae (SNe) is triggered by the collapse of massive stars (Burbidge et al. 1957). As the stellar core collapses its gravitational energy is released through the emission of neutrinos (Colgate & White 1966; Bethe 1990). A small fraction of these neutrinos are absorbed and the heating this provides drives the supernova explosion. Prior to the appearance of supernova 1987A, this mechanism, though well-developed, had no direct observational validation. The observation of neutrinos from SN 1987a

at both the IMB (Bionta et al. 1987) and Kamiokande (Hirata et al. 1987) detectors provided the first such validation. Both the ~ 2 s duration of the neutrino burst and the number flux of neutrinos agree well with the predictions of the core-collapse model. However, with all the reassurances SN 1987A provides in support of the standard model, it also brings many new puzzles. One such unsolved mystery is the lack of detection of the neutron star formed during the collapse.

Neutron stars formed in type II supernovae are thought to emit radiation as pulsars, the Crab pulsar (Rickett & Seiradakis 1982) being the canonical example. Even if the pulsar were not directed along our line of sight, its radiation would heat the surrounding supernova remnant and add to its bolometric luminosity. At present, all of the luminosity of SN 1987A can be accounted for by a radioactive decay model (with corrections for the “freeze-out” of the ionization state at late times) consistent with the production of $0.075M_{\odot}$ of ^{56}Ni (Kozma & Fransson 1998). The current lack of evidence of any “additional” energy source places a limit on any emission from the pulsar in SN 1987A at $\sim 10^{37}\text{erg s}^{-1}$ (Suntzeff et al. 1992, Kozma & Fransson 1998), a factor of 50 times lower than that of the Crab pulsar.

Where, then, is the neutron star formed by SN 1987a? First, it may not be a pulsar. SN 1987A’s remnant may have a magnetic field which is too weak, or it may not be spinning sufficiently rapidly, to drive a strong pulsar like that in the Crab. Alternatively, the neutron star could be obscured by material which is falling back onto the neutron star. Even so, one would expect accretion to provide a sufficient energy source to have been observed (Woosley, Hartman, & Pinto 1989). Houck & Chevalier (1991) have shown that the ever-present fallback of matter onto the neutron star (Woosley & Weaver 1995) would produce a luminosity roughly equal to the Compton Eddington Luminosity ($L_{\text{Edd},e^-} = 4 \times 10^{38}\text{erg s}^{-1}$), over an order of magnitude greater than the observed limit of 10^{37}erg s^{-1} .

It would seem we are forced to accept that the neutron star in SN 1987A must have collapsed further into a black hole whose accretion luminosity might be below the observational limits. Although the duration of the neutrino burst from 1987A precludes further collapse during the first ~ 20 seconds, the neutron star may have collapsed into a black hole at some later time due either to the accretion of a sufficient fall-back mass and/or to some change in its equation of state.

The late-time fallback calculated by Woosley & Weaver (1995) could, presumably, push the neutron star beyond the critical mass, forcing it to collapse into a black hole. However, their calculations estimate typical fallback masses given the likely SN 1987A progenitors to be $\sim 0.2M_{\odot}$ and total neutron star remnant gravitational masses $\lesssim 1.7M_{\odot}$. In fact, because $0.07M_{\odot}$ of ^{56}Ni was certainly ejected from SN 1987a, the maximum mass of its compact remnant cannot be greater than this value or it would have accreted all of the ^{56}Ni production. If this low-mass neutron star did indeed collapse into a black hole, many of the current equations of state for dense matter must be incorrect. Bethe & Brown (1995) have used the collapse of the neutron star initially formed in SN 1987A to argue for an equation of state softened by pion condensates. Such an exotic equation of state, or something akin to it, is required to explain such a low stable mass for neutron stars.

The news of the demise of 1987A’s neutron star may be premature, however. In this paper, we study the characteristics of the fallback material to question the high accretion luminosity derived by Houck & Chevalier (1992). Their result is based on the assumption that the opacity of the fallback material is comparable to Compton scattering. We show in this paper that for conditions appropriate to many fallback scenarios, the actual opacity can be more than 3-4 orders of magnitude greater than that due to Compton scattering alone, both in the first few days past explosion and for many years thereafter. The appropriate “Eddington limit” for the accreting neutron star is thus over three orders of magnitude lower than that

employed by Houck & Chevalier (1992) and would likely remain undetectable in the lightcurve of SN 1987A for centuries to come. Indeed, in our simulations the accreting material drives a photon wind which halts further accretion, leaving a bare neutron star on timescales of less than a year. If the compact remnant of 1987A has not yet formed a strong pulsar, it may still be a neutron star.

We first calculate the effect of this high opacity on the evolution of an atmosphere formed by the fallback process. In §2, we discuss the nature and effects of the fallback which occurs during the supernova explosion as the shock progresses through the hydrogen envelope, sending a reverse shock back toward the nascent neutron star and driving very rapid accretion $\dot{M} > 10^4 M_\odot \text{yr}^{-1}$ (Woosley & Weaver 1995). The structure of this atmosphere is derived in §2.1 and compared (favorably) to the numerical calculations in §2.2. Most of the atmosphere is accreted via neutrino emission leaving an atmosphere which cools through photon diffusion. However, the opacity of the outer layers of this atmosphere is 3-4 orders of magnitude higher than that of electron scattering and is dominated by recombined heavy elements. These outer “blanket” layers are blown off as a wind driven by the flux diffusing from the inner, hotter (dissociated), and consequently lower-opacity layers at the Compton Eddington rate (§2.3). This energy flux, derived from the gravitational energy of the accreting matter, goes primarily into reducing the gravitational binding energy of the ejected matter and produces a photon flux nearly 3 orders of magnitude below the detection limit. This process continues until all the matter in the atmosphere is either accreted or ejected.

Although numerical considerations limit our calculations to only a small fraction of the duration of this process, the outcome of the process is not in doubt. In a relatively short time, hours to weeks after neutrino cooling has shut down, the photon heat flow at L_{Edd,e^-} at the base of the atmosphere is sufficient to remove all the mass of the initial atmosphere. Further accretion could occur at later times (say 10 years after the supernova event) and understanding its fate and the luminosity it produces requires a more detailed discussion of line driven opacity, which we relegate to §3. Here again, we find the accretion luminosity to be much less than the Compton Eddington rate. Line-driven opacity dominates the opacity in all fallback accretion scenarios, and the resultant luminosities are below the current detection threshold. A neutron star may yet lurk in the ashes of SN 1987A.

2. Supernova Fallback

The first calculations of fallback in supernovae occurred soon after the initial proposal of the neutrino-driven supernova mechanism (Colgate 1971, Bisnovatyi-Kogan & Lamzin 1984). In these calculations, the fallback results from the loss in pressure support of the expanding ejecta as the material near the neutron star quickly cooled through neutrino emission. Lacking pressure support, the matter falls back onto the neutron star because of the strong gravitational field. In this mechanism, material began to fall back onto the neutron star almost immediately after the launch of the supernova explosion. Since this time, a new mechanism causing fallback at later times ($10 - 10^4$ s after the explosion) was discovered through simulations of 1987A supernova explosions (Shigeyama et al. 1988; Woosley 1989). This fallback arises from a deceleration of the inner layers of the explosion. As the initial explosion shock encounters the massive envelope of the star, material piles up behind it, sending a pressure wave (a shock in most simulations) back toward the center and decelerating the inner layers, driving material back onto the nascent neutron star (Herant & Woosley 1994; Woosley & Weaver 1995).

Figure 1 shows the rate of mass infall from fallback for three different supernova models calculated from the simulations of Woosley & Weaver (1995). Note that the bulk of the accretion occurs at very rapid

infall rates ($\gtrsim 10^4 M_\odot \text{y}^{-1}$). The fate of fallback material with these infall rates has been studied in detail (Chevalier 1993, 1996; Houck & Chevalier 1992; Brown 1995; Fryer, Benz, & Herant 1996). Above a critical infall rate $\sim 10^{-4} M_\odot \text{y}^{-1}$, this material cools quickly through neutrino emission and accretes onto the neutron star. Below this, photon radiation dominates the cooling of the infalling material and the photon Eddington limit becomes important. All of these calculations, however, assume a constant infall rate which is clearly not appropriate at later times.

In this section we are interested in the structure of the atmosphere which remains around the neutron star after neutrino cooling becomes inefficient and, hence, must accrete through photon cooling. This material is comprised of the last bit of fallback onto the neutron star at times when the infall rate is decreasing rapidly (see Figure 1). We derive the structure equations of the atmosphere for a variable infall rate, ultimately deriving not only the density and temperature profiles but also the amount of mass that piles on top of the neutron star. We compare these semi-analytic results to those of detailed hydrodynamical simulations.

2.1. Structure Equations

The characteristics of an accretion shock for a constant infall rate are well known (e.g. Chevalier 1993). In the strong shock limit for a radiation-pressure dominated ($\gamma = 4/3$) gas, the pressure (P_{sh}), density (ρ_{sh}), and hence, entropy (S_{sh}) at the shock are given by:

$$P_{\text{sh}} = 7/6 \rho_{\text{ff}} V_{\text{ff}}^2, \quad (1)$$

$$\rho_{\text{sh}} = 7 \rho_{\text{ff}}, \quad (2)$$

and

$$S_{\text{sh}} = P_{\text{sh}}^{3/4} / \rho_{\text{sh}}, \quad (3)$$

where $V_{\text{ff}} = \sqrt{2GM_{\text{NS}}/R_{\text{sh}}}$ is the free-fall velocity, $\rho_{\text{ff}} = \frac{\dot{M}}{4\pi R_{\text{sh}}^2 V_{\text{ff}}}$ is the density of the accreting matter, G is the gravitational constant, M_{NS} is the neutron star mass, and R_{sh} is the shock radius. We parameterize the variable accretion rate as an exponential decrease in time, $\dot{M} \equiv \dot{M}_0 (t/t_0)^{-\alpha}$. By setting $t = t_{\text{ff}}$, we can write the infall rate as a function of radius:

$$\dot{M} = \dot{M}_0 \left(\frac{2}{\pi} G^{1/2} M_{\text{NS}}^{1/2} t_0 \right)^\alpha R_{\text{sh}}^{-3/2\alpha}. \quad (4)$$

Using these equations, we can express the entropy of the shock as a function of radius:

$$S_{\text{sh}} = 3.2 \times 10^{-18} \dot{M}_0^{-1/4} M_{\text{NS}}^{(7-\alpha)/8} \left(\frac{6.1 \times 10^3}{t_0} \right)^{\alpha/4} R_{\text{sh}}^{3/8(\alpha-1)} = S_0 R_{\text{sh},6}^{3/8(\alpha-1)} \quad (5)$$

where \dot{M}_0 , M_{NS} , and t_0 are all given in cgs units and $R_{\text{sh},6}$ is the shock radius in units of 10^6cm . All previous work assumed a constant accretion rate ($\alpha = 0$) and the resulting atmosphere was convectively unstable ($\partial S / \partial R = -\frac{3}{8} S_0 R_{\text{sh}}^{-11/8} < 0$).

Convection will strive to flatten a negative entropy profile, and for the cases where $\alpha < 1$, the entropy of the resulting accretion atmosphere (within the shock) is constant. By assuming pressure equilibrium for these constant entropy atmospheres and a neutron star mass much greater than the mass of the surrounding atmosphere, the pressure gradient is given by (see, for example, Colgate, Herant, & Benz 1993):

$$dP/dR = -g\rho = -M_{\text{NS}}G\rho/R^2. \quad (6)$$

Since the entropy is independent of radius, we can integrate equation (6) to obtain:

$$P = \left[\frac{1}{4} M_{\text{NS}} G S_0^{-1} (1/R - 1/R_{\text{out}}) + P_{\text{out}}^{1/4} \right]^4, \quad (7)$$

where R_{out} and P_{out} are the radius and pressure of the outer boundary of the atmosphere. Since we define the atmosphere as the material within the accretion shock, R_{out} is equivalent to the accretion shock radius and P_{out} is the pressure at that radius. Using this relation for a radiation-dominated gas of pressure $P = 1/3aT^4$ and entropy $S = 4/3aT^3/\rho$, one can derive the structure equations for the atmosphere (Colgate, Herant, & Benz 1993)¹ including the density and temperature profiles as well as the atmosphere mass.

For the fallback scenarios we consider, as the last bit of material falls onto the neutron star, the fallback rate decreases dramatically: $\alpha > 1$ (see Figure 1). Although convection will not flatten the entropy profile for these systems, we can still derive the structure equations for these atmospheres assuming that as the shock moves outward, the entropy profile is maintained. Then, again by assuming pressure equilibrium, we can derive the pressure profile of the atmosphere:

$$P = \left[\frac{1}{4} M_{\text{NS}} G S_0^{-1} \left(R^{-5/8-3\alpha/8} - R_{\text{out}}^{-5/8-3\alpha/8} \right) + P_{\text{out}}^{1/4} \right]^4. \quad (8)$$

R_{out} is generally much beyond the regions that we consider ($R_{\text{out}} \approx R_{\text{Bondi-Hoyle}}$) and hence it and the outer pressure can be neglected. The structure equations then become:

$$P = \left[\frac{1}{4} M_{\text{NS}} G S_0^{-1} \right]^4 R^{-5/2-3\alpha/2} = P_0 R_6^{-5/2-3\alpha/2} \text{ g cm}^{-1} \text{ s}^{-2}, \quad (9)$$

$$T = \left(\frac{3}{a} \right)^{1/4} \left[\frac{1}{4} M_{\text{NS}} G S_0^{-1} \right] R^{-5/8-3\alpha/8} = T_0 R_6^{-5/8-3\alpha/8} \text{ K}, \quad (10)$$

$$\rho = S_0^{-1} \left[\frac{1}{4} M_{\text{NS}} G S_0^{-1} \right]^3 R^{-3/2(1+\alpha)} = \rho_0 R_6^{-3/2(1+\alpha)} \text{ g cm}^{-3}, \quad (11)$$

and

$$M_{\text{encl}} = \frac{4\pi}{3/2(1-\alpha)} S_0^{-1} \left[\frac{1}{4} M_{\text{NS}} G S_0^{-1} \right]^3 \left[R_{\text{NS}}^{3/2(1-\alpha)} - R_{\text{max}}^{3/2(1-\alpha)} \right] M_{\odot}, \quad (12)$$

where R_{NS} is the radius of the neutron star and R_6 is the radius in units of 10^6 cm. In next section, we compare this analytic derivation of the atmosphere's structure to those calculated by numerical simulation. These analytic results will give us a basis from which we can build our understanding of the evolution of these atmospheres.

2.2. Comparison to Simulations and the Atmosphere Mass

The structure equations do not uniquely define the atmosphere around the neutron star. They depend both upon the parameter α and the initial accretion rate $\dot{M}_0 t_0^\alpha$. Although the uncertainty in fallback rates

¹Our derivation differs from the work of Colgate, Herant, & Benz (1993) in that we assume we can neglect the effects of electron-positron pairs. For the temperatures involved in this work, this assumption is valid.

allows relative freedom in the choice of α , we can constrain $\dot{M}_0 t_0^\alpha$ by insisting that we consider only the mass of the atmosphere which is not cooled primarily by neutrinos. The neutrino cooling of the atmosphere at temperatures $\lesssim 1$ MeV is dominated by electron capture on protons and can be approximated by (Bethe 1990):

$$L_\nu = \int_{r=R_{\text{NS}}}^{\infty} 2 \times 10^{18} T_{\text{MeV}}^6 \rho 4\pi r^2 dr \text{ erg/s.} \quad (13)$$

By setting the neutrino luminosity equal to the Compton Eddington luminosity ($L_{\text{Edd},e^-} \approx 4 \times 10^{38} \text{ erg s}^{-1}$; the material is still fully ionized), we estimate the temperature at the base of the atmosphere to be $\sim 0.4 \text{ MeV}^2$. As the temperature drops to $\sim 0.2 \text{ MeV}$, the neutrino luminosity becomes negligible ($< 10^{-3} L_{\text{Edd},e^-}$). Choosing a neutrino luminosity, we can then iteratively derive the temperature at the surface of the neutron star (T_{NS}) and the value of the initial accretion rate $\dot{M}_0 t_0^\alpha$ for a given α . Using this relation, we can derive ρ_0 , P_0 , and M_{atm} . Hence, the structure of our photon-cooling atmosphere is uniquely defined by a given α .

Our simulations (see the appendix for a description) model both neutrino emission and absorption as well as photon transport. We set up a range of infall initial conditions by varying α and allowing the matter to build an atmosphere around the neutron star. If the material begins to cool significantly through neutrino emission, it compresses above a critical density and we accrete it onto the neutron star, removing it from the atmosphere. The atmosphere which remains will persist until it can be accreted via photon emission. In this section, we will discuss the structure of this remaining atmosphere.

Figure 2 shows the simulated fallback profiles (for $\alpha = 1.5$, ~ 30 s after the initial fallback) of density, temperature, pressure, and entropy and the corresponding profiles of these quantities from equations (5, 9-11). The entropy gives the best indication of the fit as it does not vary so dramatically with radius. Figure 3 shows entropy profiles ~ 30 s after the initial fallback for a series of atmospheres varying α . Our analytic description of the atmosphere agrees well with the simulations until the material becomes sufficiently transparent to photons that the effects of photon diffusion become important.

At this point in the simulations, the density and temperature structure of the atmosphere near the base of the neutron star is well defined and we can determine much of the internal structure of the atmosphere. Table 1 gives the derivations of P_0 , T_0 , and ρ_0 for a range of values for α which, combined with equations (9-11), defines the internal structure of the atmosphere. We will use these properties in §2.3 to discuss the late-time evolution of the atmospheres. Table 1 lists both the analytic estimate of the total enclosed mass for each atmosphere and that obtained through simulations. For comparison with the simulations, we list simulation results when $L_\nu = 10^5 L_{\text{Edd},e^-}$. The table also includes the data for a neutrino luminosity of L_{Edd,e^-} for several values of α . The accretion timescale (t_{acc}),

$$t_{\text{acc}} = \frac{GM_{\text{NS}}M_{\text{atm}}}{r_{\text{NS}}\max(L_\nu, L_{\text{Edd},e^-})}, \quad (14)$$

increases dramatically as the atmosphere cools and can be as high as $\sim 10^6$ s when the neutrino luminosity equals the Compton Eddington luminosity.

Most of the material quickly cools and accretes via neutrino emission. Although the cooling time is proportional to the binding energy, and hence mass, of the atmosphere, the strong dependence of the

²This critical temperature depends upon α and for each atmosphere we must calculate the exact critical base temperature. However, the strong dependence of the neutrino luminosity on temperature prevents significant deviation from 0.4 MeV.

neutrino cooling on the temperature, $\propto T^9$, causes the last bit of material to take the longest to accrete. The temperature at the base of the atmosphere $T_0 \propto M_0^{1/4}$ (eqs. 10,12) and neutrino cooling, then, is roughly proportional to $M_0^{9/4}$. The mass at which $L_\nu = L_{\text{Edd},e^-}$ defines a sharp boundary between rapid neutrino cooling above and constant cooling due to photons below this condition. Because the neutrino cooled phase is so rapid, we can estimate the total accretion timescale to be equal to the accretion timescale at this critical mass.

2.3. Post-Fallback Evolution

Returning to our discussion of the neutron star atmosphere, as the temperature at the base of the atmosphere drops below $\sim 0.4\text{MeV}$, the neutrino cooling becomes negligible. At this point, the cooling of the atmosphere depends almost entirely upon the photon heat transport. If the dominant opacity source were electron scattering, the luminosity of the accreting neutron star would roughly equal the usual Compton Eddington luminosity. The strong dependence of the opacity on temperature as the temperature drops below 0.2 keV creates a narrow transition region from electron-scattering to an opacity dominated by recombined heavy elements, especially those of the iron group (see Figure 4). Thus, where the temperature drops below this value, there is a narrow transition region within which the Eddington limit falls dramatically.

Figure 5 shows the luminosity profile for a simulation with $\alpha = 1.1$ as a function of time. The region whose opacity is dominated by iron³ forms an insulating blanket around the atmosphere, limiting its cooling rate. At this boundary, photon pressure halts the infall and eventually drives off the fallback material in a wind. Almost all of the photon energy generated below this opacity boundary, at the Compton L_{Edd,e^-} , goes into ejecting mass, doing work against its gravitational binding; in other words, the accretion flow bifurcates, the outer layers reversing direction and forming a wind. Because the accretion rate (from larger radii) has fallen nearly to zero by this time, this wind meets virtually no resistance and is driven off to “infinity”.

Figure 6 shows mass-point trajectories for a typical simulations ($\alpha = 1.1$). Much of the matter accretes onto the neutron star, while the rest is driven off in a wind. The atmosphere is removed over a cooling timescale ($\lesssim 10$ days – see Table 1). As the atmosphere expands in response to the decreased pressure of its diminishing outer layers, the temperature decreases in deeper layers. These layers then also recombine and, in turn, are driven off. This process continues until the atmosphere either accretes onto the neutron star or is blown off in the accretion-driven wind.

During this late phase, the observable luminosity of the accreting neutron star is the fraction of the photon emission which escapes conversion into kinetic energy in the “blanket” – i.e. the iron-opacity Eddington limit. Figure 7 shows the photon luminosity at infinity throughout the accretion process; after about 500 seconds the luminosity is seen to fall by the expected 3 to 4 orders of magnitude. Any subsequent accretion will continue to produce a luminosity limited to $\lesssim 10^{-3}$ of the fully-ionized Compton Eddington limit.

We have thus established that after a very brief interval, essentially none of the original fallback is left to accrete onto the neutron star at later times.

³In the regimes that are most important for our fallback simulations, the results do not change significantly (30 %) if the fallback material were instead composed entirely of oxygen.

3. Fallback Accretion 10 Years After

We have shown in §2 that any of the “late-time” fallback predicted by Woosley & Weaver (1995) is removed within a year of the supernova explosion. But what about 10 years later for the case of SN 1987A? Present calculations of fallback (e.g. Woosley & Weaver 1995) can tell us little about very low rates of accretion. The Compton Eddington accretion limit is only $10^{-8}M_{\odot} \text{ y}^{-1}$; such a small value is far below the resolution limit of present-day hydrodynamic calculations (being much less than a single zone per year in the current fallback simulations). It is not at all unreasonable to expect that, while the accretion rate declines rapidly to such small values, it may remain at such values for periods of up to many years.

For example, years after the explosion, the decay of ^{56}Ni in the supernova may decelerate some of the innermost material to the point where it becomes once again gravitationally bound to the neutron star. The energy available from radioactive decay of ^{56}Ni to ^{56}Fe ($9.3 \times 10^{16} \text{ erg g}^{-1}$) corresponds to a velocity increment of 4300 km s^{-1} and this energy will both accelerate the outer mass *and* decelerate the inner region of the supernova ejecta.

By extrapolating the results from Woosley & Weaver (1995), we can estimate the accretion rate, and hence potential energy from accretion released from fallback years after the supernova event. If we take an arbitrary ejecta velocity of the inner zone from the simulations by Woosley & Weaver ($\sim 10^{-3}M_{\odot}$) to be 100 km s^{-1} , after 1000 days its radius is $\sim 10^{15} \text{ cm}$. At these times, the density of this inner material has decreased to $\sim 10^{-15} \text{ g cm}^{-3}$. Due to the homologous outflow which characterizes supernova explosions, the outer material has expanded at even higher velocities and the density decreases sharply with radius. If this inner zone were to decelerate and become bound to the neutron star, it would accrete roughly over a free fall time, and the accretion rate ($\dot{M} = M_{\text{inner zone}}/t_{\text{free fall}}$) would be $\sim 10^{-13}M_{\odot} \text{ s}^{-1}$. The potential energy released during this time yields a luminosity $\sim 3 \times 10^{33} \text{ ergs}^{-1}$, 4 orders of magnitude below the detection threshold.

However, we can only make rough estimates given the current resolution of the simulations and we can not preclude accretion rates of $\sim 10^{-9}M_{\odot} \text{ s}^{-1}$. Such small accretion rates, if all their accretion energy were converted to photons, would be detectable above the standard decay light curve of SN 1987A. In this section, we direct our attention to the possibility that accretion rates as high as $\sim 10^{-9}M_{\odot} \text{ s}^{-1}$ might occur after 10 years.

Since the composition of this late-time fallback will still be representative of the innermost layers of the ejecta, it will still have an opacity which is dominated by heavy elements and thus have an Eddington limit far below the Compton value. Just as in §2 where the iron opacity converted most of the potential energy of the accreting material into kinetic energy of an accretion driven wind, we find that even after 10 years, line-driven opacity will limit the accretion rate. However, we now move into regimes where the SESAME opacity table is no longer accurate and must, in this section, discuss the fundamentals of line-driven opacity and apply their consequences on the emission from this additional fallback.

3.1. Line-Driven Opacity

The increase in mean opacity above the Thomson opacity is a simple consequence of atomic physics. The Thomas-Rieche-Kuhn sum rule requires that the sum over all the oscillator strengths f_{ij} of transitions arising from a given atomic level equals the number of electrons which participate in giving rise to the transitions from that level. Most often, this just means that the sum of all the f_{ij} over all transitions

arising from a given level equals unity. Since the sum over all of the populations of all levels in an ion must equal the density of the ion, the sum of all the oscillator strength in an ion must be equal to the number of bound electrons. How, then, does having a large number of transitions in the spectrum of an ion increase the radiation force above that for Thomson scattering?

The answer is that the “oscillator strength” of a free electron is spread out over (nearly) all energies, while the effect of atomic physics is to concentrate the oscillator strength within a relatively narrow range of energies, characteristically within a factor of ten of the ground-state ionization threshold. If this range of energies coincides with that of the radiation field (so that the Rosseland mean weights it most heavily), the mean opacity can then be greatly increased. Further, if the matter and radiation temperatures are not too dissimilar, the dominant ionization stages will always occur such that the peak of the radiation field is close to the typical energy of the most important transitions.

Thus, as soon as the material in the atmosphere begins to recombine, it’s opacity rises sharply. This effect is strengthened at high densities by pressure broadening. The strong lines in the spectrum are nearly black at their cores, and pressure broadening allows each line to absorb a greater fraction of the spectral bandwidth. At densities below which pressure broadening has a significant effect, the opacity can still be increased by the presence of a velocity gradient in the flow – the spread of co-moving frame energies “seen” by a photon with fixed observer-frame energy again allows a single optically thick line to absorb greater fraction of the total bandwidth.

The effect of pressure broadening is included in the high-density opacities we have employed from the SESAME code (Magee 1993). At densities below $\sim 10^{-11}\text{g cm}^{-3}$ and temperatures below $\sim 1\text{eV}$ these opacities become unreliable due to incompleteness in the atomic physics calculations. At significantly higher densities, the effects of a velocity gradient, which are not included in the SESAME data, have already become important. We therefore take the larger of the results from the SESAME tables or the “expansion opacity” described in the following sections.

In the SESAME opacities employed above, for temperatures near 0.1 MeV the main contribution arises from bound-free transitions and lines significantly broadened by the high density. Further out in the flow, at lower temperatures and densities, the ions become more recombined and lines begin to dominate the opacity. Because of the density of lines in iron-group elements, the opacity is strongly increased by a velocity gradient – the larger the velocity gradient ($\propto t^{-1}$ for homologous expansion), the greater its opacity and the lower the Eddington limit. Even for Fe II at nebular temperatures, the Eddington limit in the inner layers of the ejecta is much reduced below the electron-scattering value. Thus, even for very cool material far from the neutron star, matter is accelerated outward by a luminosity below observational limits. We argue that any possible accretion rate is thus severely limited.

3.2. Heating and Momentum Transfer

There are two ways in which an increased opacity can affect an accretion flow. The first is by increasing the heating rate in the high-opacity material. In the diffusion limit, if the flow is to sustain a given luminosity it must achieve a sufficient temperature gradient to overcome the effect of the opacity by heating the inner parts of the high-opacity region.

As we have shown in §2, the entropy profile that develops for these fallback atmospheres is convectively stable (see Figures 2,3). As long as the accretion rate falls off rapidly ($\alpha > 1$), the atmosphere will not be

convectively unstable. However, in the innermost parts of the high-opacity region, the increased heating rate raises the entropy and initiates convection. In our simulations of the initial fallback, this entropy gain was limited to the inner zone of the high-opacity region and the resultant convective region would lie in a very narrow radial space.

Even if the boundary between the high- and low-opacity regions is disrupted by an instability, beyond the unstable region the radiation field can *still* not be greater than the appropriate Eddington limit. The accretion flow will be stopped by radiation pressure at the *largest* radius at which the radiation force exceeds gravity. As one moves outward in radius, the flow can be expected to become more uniform and the radiation field more spherically symmetric, so that at such radii the usual Eddington argument still applies. Thus, the detailed nature of the flow near the neutron star seems not to be crucial to our argument.

3.3. The Eddington Limit for a Line-Dominated Opacity

An increased opacity can also increase the rate of momentum transport from the radiation field to the gas. The spherically-symmetric gas momentum equation in the co-moving frame is, to $O(v/c)$,

$$\rho \frac{Dv}{Dt} = -\frac{GM(r)\rho}{r^2} - \frac{\partial p}{\partial r} + \frac{1}{c} \int_0^\infty F_\nu \chi_\nu d\nu \quad (15)$$

The last term is the radiation force per unit volume (or momentum flux per unit length), where χ_ν is the extinction coefficient (units: length⁻¹).

In the usual treatment of the Eddington limit, the opacity is taken to be due only to free electrons, $\chi_{e^-} = \rho N_A f \sigma_e / \bar{A}$, where f is the mean number of free electrons per ion, \bar{A} is the mean atomic weight of the material, and σ_e is the Compton cross section at the flux-weighted mean energy of the radiation field. Assuming a radially-streaming radiation field with total flux F , we have the radiation force

$$\phi_{e^-} = \frac{F \rho N_A f \sigma_e}{c \bar{A}} \quad (16)$$

or $\phi_{e^-} = 1.3 \times 10^{-11} \rho F f / \bar{A}$ in cgs units in the low-energy (Thomson) limit.

If we set $F = L/4\pi r^2$ and ignore the gas pressure gradient, equation (15) gives us the usual Eddington limit

$$L_{\text{Edd},e^-} = 1.25 \times 10^{38} \left(\frac{M}{M_\odot} \right) \frac{\bar{A}}{f} \text{ergs}^{-1} \quad (17)$$

This limit is an absolute upper bound on the photon luminosity generated by accretion in a steady state, spherically symmetric flow. Above this limit the radiation force on the free electrons alone exceeds gravity. Without neutrino cooling, accretion cannot take place at rates much larger than this value. Even where neutrino cooling is important, the excess photon luminosity above the Eddington limit will drive mass outflow, and the photon luminosity at infinity will fall near or below the limit. For once-ionized material dominated by iron-group elements, as expected for the inner layers of the ejecta, we have $L_{\text{Edd},e^-} \sim 7 \times 10^{39} (M/M_\odot) \text{erg s}^{-1}$, or about $10^{40} \text{erg s}^{-1}$.

We have already discussed the increased opacity at high densities immediately after fallback. In the supernova ejecta at late times the effective opacity will also be much larger at nebular temperatures and the Eddington limit will again be correspondingly much lower. Eastman and Pinto (1993) give an expression

for the opacity of a large number of lines (the “expansion opacity”) in the Sobolev limit as

$$\chi_\nu = \nu \frac{\beta}{r} \frac{\sum_j \int_0^1 (1 + Q\mu^2) \{1 - e^{-\tau_j(\mu)}\} d\mu}{\Delta\nu}, \quad (18)$$

where for an outflow the sum extends over all lines in the interval $[\nu, \nu + \Delta\nu]$. μ is the direction cosine from the radial direction, and $\tau_j(\mu)$ is the Sobolev optical depth of line j in the direction μ ,

$$\tau_{lu}(\mu) = \frac{h}{4\pi} \frac{n_l B_{lu} - n_u B_{ul}}{|\partial\beta/\partial l|}, \quad (19)$$

or, neglecting stimulated emission,

$$\tau_{lu}(\mu) = \frac{\pi e^2}{m_e c} \nu_{lu}^{-1} f_{lu} n_l \left| \frac{\partial\beta}{\partial l} \right|^{-1}, \quad (20)$$

where f_{lu} is the oscillator strength of the transition and the directional derivative is

$$\frac{\partial\beta}{\partial l} = \frac{\partial\beta}{\partial r} (1 + Q\mu^2), \quad (21)$$

with

$$Q = \frac{\partial \ln \beta}{\partial \ln r} - 1. \quad (22)$$

Q is zero for homologous flow (throughout most of the ejecta in the supernova), and takes on a value of $-3/2$ for free infall.

Following the discussion in Eastman & Pinto (1993), the integral over angle

$$I_j = \int_0^1 (1 + Q\mu^2) \{1 - e^{-\tau_j(\mu)}\} d\mu \quad (23)$$

has the limits $(1 + Q/3)$ for $\tau_j(\mu = 0) \gg 1$ and $\tau(1 + \tau Q/3)$ for $\tau_j(\mu = 0) \ll 1$. We will approximate the integral as

$$I_j = \tau^* \left(1 + \frac{\tau_j^* Q}{3} \right) \quad (24)$$

with $\tau_j^* = \min(\tau_j(\mu = 0), 1)$. This gives us the opacity

$$\chi_\nu = \nu \frac{\beta}{r} \frac{\sum_j \tau^* (1 + \tau_j^* Q/3)}{\Delta\nu}. \quad (25)$$

The value of this opacity clearly depends upon knowing the spectral density of line transitions: the number of lines per unit frequency. While line lists are available from which we can determine the spectral density, most such lists are seriously incomplete, especially in the context of heavy-element-rich supernova ejecta. As a purely illustrative example, we have employed the line list of Kurucz (1991) which lists roughly 171,000 lines of Fe and Co with lower-level energies of 10^5cm^{-1} or less. The true value of the opacity will be rather larger due to the incompleteness of the list.

We have assumed an LTE equation of state at a temperature of 5000K. Such a temperature is typical of models for supernova ejecta at times later than a few hundred days. The matter is assumed to be expanding homologously ($\partial v/\partial r = v/r = 1/t$) and has a density scaled from the inner zones of hydrodynamic simulations. We have chosen a density range with $\rho = 10^{-8} - 10^{-6} \text{g cm}^{-3}$ as being typical. Figure 8 shows

the computed Eddington limits from this model. At present (10 years past explosion), the Eddington limit is near if not below the observational limit. Calculations, such as those of Woosley & Weaver (1995), show a density near $5 \times 10^{-7} \text{g cm}^{-3}$ (scaled to one day) in their innermost zones, but the density profile from these simulations falls off very strongly with decreasing radius and the mass resolution of the innermost zone only $\sim 10^{-3} M_{\odot}$ which makes it difficult to determine the density profile. Unfortunately, without far more detailed simulations of the dynamics of the innermost portion of the ejecta, a firm prediction of whether the ejecta Eddington limit is below the observed luminosity is impossible.

If the neutron star is given a significant impulse (“kick”) during the explosion, it will find itself moving with the flow at the same velocity. Thus, the material surrounding it will have zero velocity in its own frame. Because the velocity gradient in homologous expansion is isotropic, the flow will still be isotropically outward from the neutron star, and the arguments of this section will remain valid.

4. The remnant of SN 1987a

We have shown that virtually all of the late-time fallback of material onto a nascent neutron star which occurs in most supernova simulations (Woosley & Weaver 1995) accretes rapidly onto the neutron star. However a small remnant of this material ($\sim 10^{-11} - 10^{-9} M_{\odot}$) remains on the neutron star and cools due to photon emission. Due to the high opacity of recombined iron, the atmosphere emits at a rate much below Compton Eddington ($\sim 10^{-3} L_{\text{Edd},e^-}$), with most of the photon energy driving a wind from the neutron star. The accretion times of the atmospheres are $\lesssim 0.1$ yr. Any further fallback will be limited to the iron-opacity Eddington accretion rate. In the case of 1987a, this means that, although we would not expect to see any luminosity from the fallback.

If no mechanism drove further fallback onto the neutron star (e.g. the decay of ^{56}Ni), then the neutron star remnant of SN 1987A should now have no obscuring atmosphere. If this did indeed occur, and if the neutron star is rotating rapidly and has a strong magnetic field (such as the Crab Pulsar), then we should observe it as a pulsar. Only when all of these “ifs” are satisfied must we, as Bethe & Brown (1995) have suggested, conclude that the neutron star has indeed collapsed into a black hole.

We acknowledge the early work of Kaiyou Chen, whose unpublished research first recognized the importance of the opacity of recombined iron. We are grateful to Stan Woosley for access to fallback models and for many discussions related to fallback and fallback rates. We would also like to thank Roger Chevalier, Adam Burrows and Willy Benz for many useful discussions on this topic. The work of C. Fryer was supported by the NSF (AST 94-17161) and by NASA (NAG5 2843 and MIT SC A 292701) and of P. Pinto by the NSF (CAREER grant AST9501634) and by NASA (NAG 5-2798). P. Pinto gratefully acknowledges support from the Research Corporation through a Cottrell Scholarship. S. Colgate acknowledges the support of LDRD funds through DOE and UC.

A. Code Description

For these simulations, we have used the one-dimensional lagrangian code tested in several previous papers (Herant et al. 1994, Fryer et al. 1996). The equation of state and the neutrino transport and emission/absorption processes are described in detail in Herant et al. (1994). In this appendix, we describe the physics added to the code to simulate late-time fallback onto neutron stars. We begin by describing our

initial conditions and how we “accreted” material onto the neutron star. We end with a discussion of our photon transport and opacity calculations.

We begin with free-fall initial conditions where the accretion rate onto the neutron star is $10^5 M_\odot \text{y}^{-1}$. This rate declines proportionally to $t^{-\alpha}$ where α is a free parameter. We use 500 zones to model the entire fallback material from 10 km - 6×10^5 km. These zones vary in size from ~ 1 km near the surface of the neutron star to $\sim 10^4$ km near the edges of our simulation. In our lagrangian code, these sizes vary during the course of the simulation, but not noticeably. As the cell next to the surface of the neutron star cools and its density increases beyond a critical density (ρ_{crit}), that cell is accreted. The value for ρ_{crit} is gradually decreased ($10^{11} - 10^5 \text{g cm}^{-3}$) during the simulation after the initial structure of the atmosphere is defined, allowing us to follow the evolution of the atmosphere to later times ($10^3 - 10^4$ s).

For photon opacity, we use the SESAME opacity data (Magee 1993) for the high density/high temperature regimes. Below a density of $10^{-11} \text{g cm}^{-3}$ or a temperature below 1eV, the SESAME data is incomplete. In this regime, we use the approximation for the expansion opacity at the Sobolev limit by Pinto (1997):

$$\chi = \frac{D\beta}{r} \tau^* \left(1 + \frac{\tau^* Q}{3} \right), \quad (\text{A1})$$

D is the number of lines per frequency bin, $\beta = \max(\text{material velocity, sound speed}) / (\text{speed of light})$, $\tau^* = \min(1, 10^{13} \rho \text{ cm}^3/\text{g})$, and $Q = \frac{\partial \ln \beta}{\partial \ln r} - 1$. The boundary between these two regimes does not reflect a smooth transition; the low-density expansion opacity approximation is lower than the predicted opacity from the SESAME data. Our low-density opacity is likely to be an underestimate, implying that our calculated photon luminosities are higher than the actual values. We have also run the same simulation assuming that the opacity remains closer to the SESAME data in the low-density regime and the photon luminosity did not decrease significantly as most of the flux is coming from the high-density regimes where we use the SESAME data.

The photon transport is modeled using the Levermore-Pomraning flux limiter (Levermore & Pomraning 1981). Our assumption that the photons are emitted in local thermodynamic equilibrium from each cell holds for most of atmosphere where the cell sizes are much longer than a few mean-free paths. In fact, if anything, the mean photon energy would be greater in the outer part of the atmosphere where the atmosphere becomes optically thin, leading to an opacity which is higher than predicted by our simulations, implying once again, that these accreting neutron stars are less luminous than we have predicted.

REFERENCES

- Bethe, H.A., 1990, Rev. Mod. Phys., 62, 801
- Bethe, H.A., & Brown, G.E., 1995, ApJ, 445, L129
- Bionta, R.M., Blewitt, G., Bratton, C.B., Caspere, D., Ciocio, A., 1987, PhRvL, 58, 1494B
- Bisnovatyi-Kogan, G.S., & Lamzin, S.A. 1984, Soviet Astron., 28, 187
- Brown, G.E. 1995, ApJ, 440, 270
- Burbidge, E.M., Burbidge, G.R., Fowler, W.A., & Hoyle, F., 1957, Rev. Mod. Phys., 29, 547
- Chevalier, R.A., 1993, ApJ, 411, L33

- Colgate, S.A. 1971, ApJ, 163, 221
- Colgate, S.A., Herant, M., & Benz, W., 1993, Phys. Reports, 227, 157
- Colgate, S.A., & White, R.H., 1966, ApJ, 143, 626
- Fryer, C.L., Benz, W., & Herant, M., 1996, ApJ, 460, 801
- Herant, M., & Woosley, S.E., 1994, ApJ, 425, 814
- Herant, M., Benz, W., Hix, W.R., Fryer, C.L., Colgate, S.A., 1994, ApJ, 435, 339
- Houck, J.C., & Cehavlier, R.A., 1991, ApJ, 376, 234
- Hirata, K.S., Kajita, T., Koshiha, M., Nakahata, M., & Oyama, Y., 1987, PhRvL, 58, 1490
- Kozma, C., Fransson, C., 1998, ApJ, 496, ???.
- Kurucz, R.L. 1991, private communication.
- Levermore, C.D., & Pomraning, G.C., 1981, ApJ, 248, 321
- Magee, N.H. Jr., 1993, Los Alamos Report LA 93-1248
- Rickett, B.J., & Seiradakis, J.H., 1982, ApJ, 256, 612
- Shigeyama, T., Nomoto, K., & Hashimoto, M., 1988, A&A, 196, 141
- Suntzeff, N.B., Phillips, M.M., Elias, J.H., Walker, A.R., & Depoy, D.L., 1992, ApJ, 384, L33
- Woosley, S.E., 1989, NYASA, 571, 397
- Woosley, S.E., & Weaver, T.A., 1995, ApJS, 101, 181
- Woosley, S.E., Hartman, D., Pinto, P.A., 1989, ApJ, 346, 395.

Table 1. Atmosphere Structure

α	S_0 ($k_B/\text{nucleon}$)	P_0 ($\text{g}/\text{cm}/\text{s}^2$)	T_0 (K)	ρ_0 (g/cm^3)	M_{atm} (M_\odot)	$M_{\text{atm}}^{\text{sim}}$ (M_\odot)	t_{acc} (10^3 s)
$L_\nu = 10^5 L_{\text{Edd}}$							
1.05	115	1.01×10^{26}	1.41×10^{10}	3.02×10^6	2.0×10^{-7}	2.1×10^{-7}	2
1.1	115	1.02×10^{26}	1.42×10^{10}	3.05×10^6	1.2×10^{-7}	1.8×10^{-7}	1
1.2	115	1.04×10^{26}	1.43×10^{10}	3.12×10^6	6.5×10^{-8}	8.4×10^{-8}	0.6
1.5	113	1.11×10^{26}	1.45×10^{10}	3.32×10^6	2.8×10^{-8}	4.4×10^{-8}	0.3
2.0	111	1.21×10^{26}	1.48×10^{10}	3.62×10^6	1.5×10^{-8}	-	0.1
3.0	107	1.37×10^{26}	1.53×10^{10}	4.12×10^6	8.6×10^{-9}	-	0.08
5.0	103	1.64×10^{26}	1.60×10^{10}	4.92×10^6	5.1×10^{-9}	-	0.05
$L_\nu = L_{\text{Edd}}$							
1.05	365	1.01×10^{24}	4.47×10^9	3.02×10^4	2.0×10^{-9}	-	2000
1.1	365	1.02×10^{24}	4.48×10^9	3.05×10^4	1.2×10^{-9}	-	1000
1.2	363	1.04×10^{24}	4.51×10^9	3.12×10^4	6.5×10^{-10}	-	600
1.5	358	1.11×10^{24}	4.58×10^9	3.32×10^4	2.8×10^{-10}	-	300
2.0	350	1.21×10^{24}	4.68×10^9	3.62×10^4	1.5×10^{-10}	-	100
3.0	339	1.37×10^{24}	4.83×10^9	4.12×10^4	8.6×10^{-11}	-	80
5.0	324	1.64×10^{24}	5.05×10^9	4.92×10^4	5.2×10^{-11}	-	50

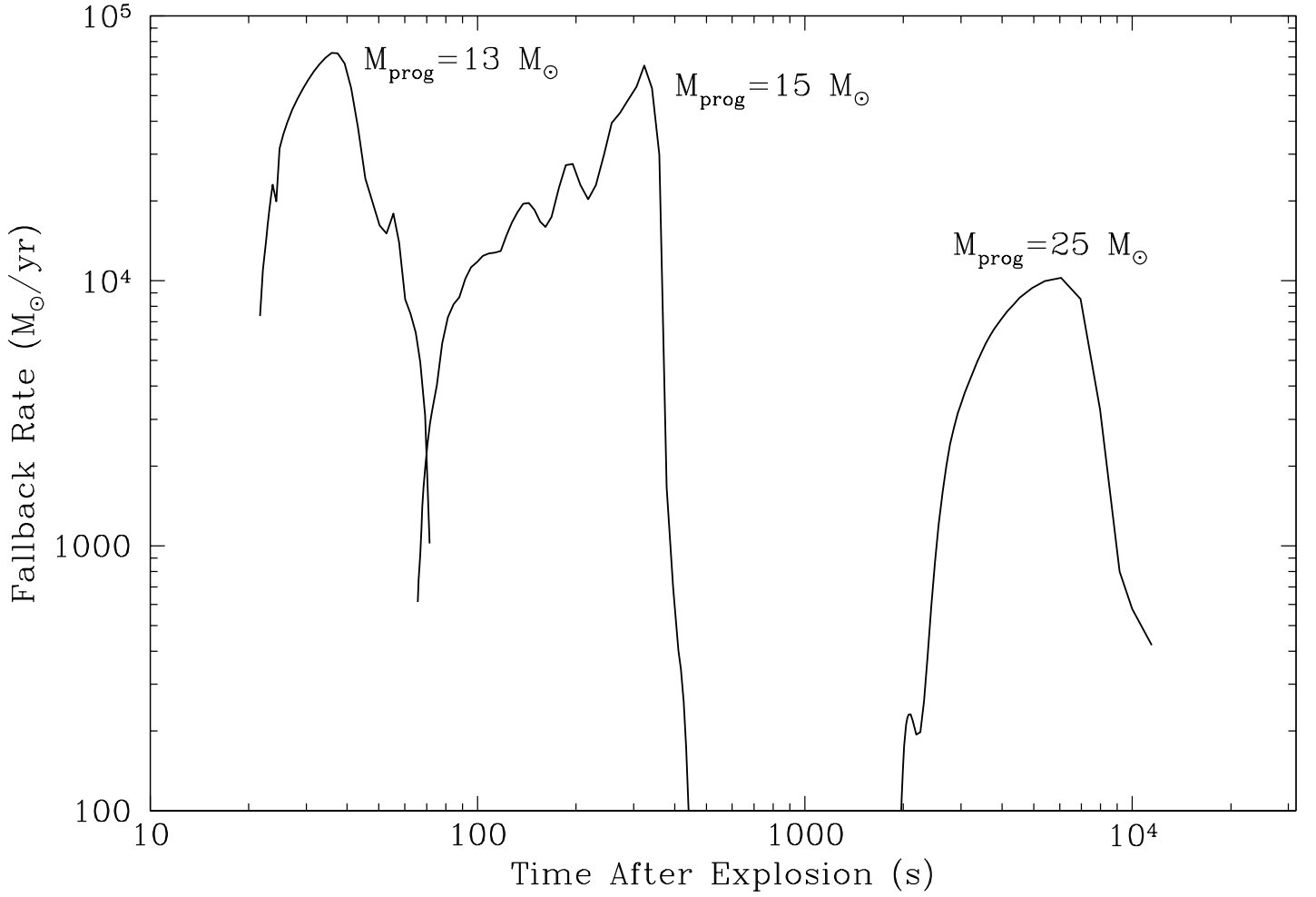


Fig. 1.— Estimated accretion rate vs. time using the models of Woosley & Weaver (1995). For all models, the accretion rate exceeds $\sim 10^4 M_{\odot} \text{yr}^{-1}$ before dropping dramatically. Most of this material will accrete via neutrino cooling. However, the last fraction of it ($\lesssim 10^{-9} M_{\odot}$) will cool due to photon emission.

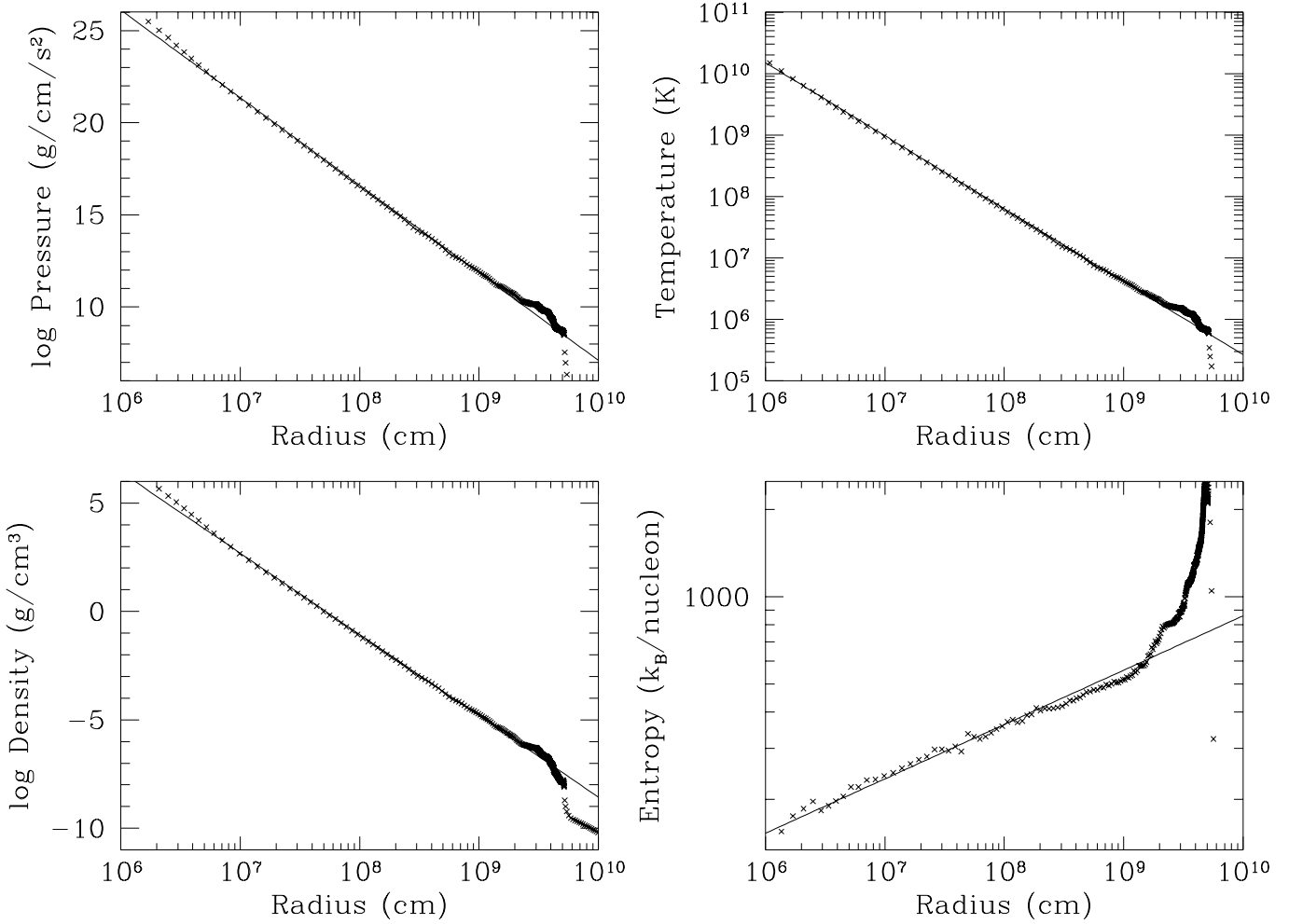


Fig. 2.— Comparison of simulations with the analytic derivation (Pressure, Density, Temperature, and Entropy) for an $\alpha = 1.5$ model. The analytic model matches the simulation well until photons are no longer “trapped” in the flow. This occurs at high enough radii that it does not effect the mass estimate for the atmosphere. Note that the Entropy is the most sensitive variable for comparison.

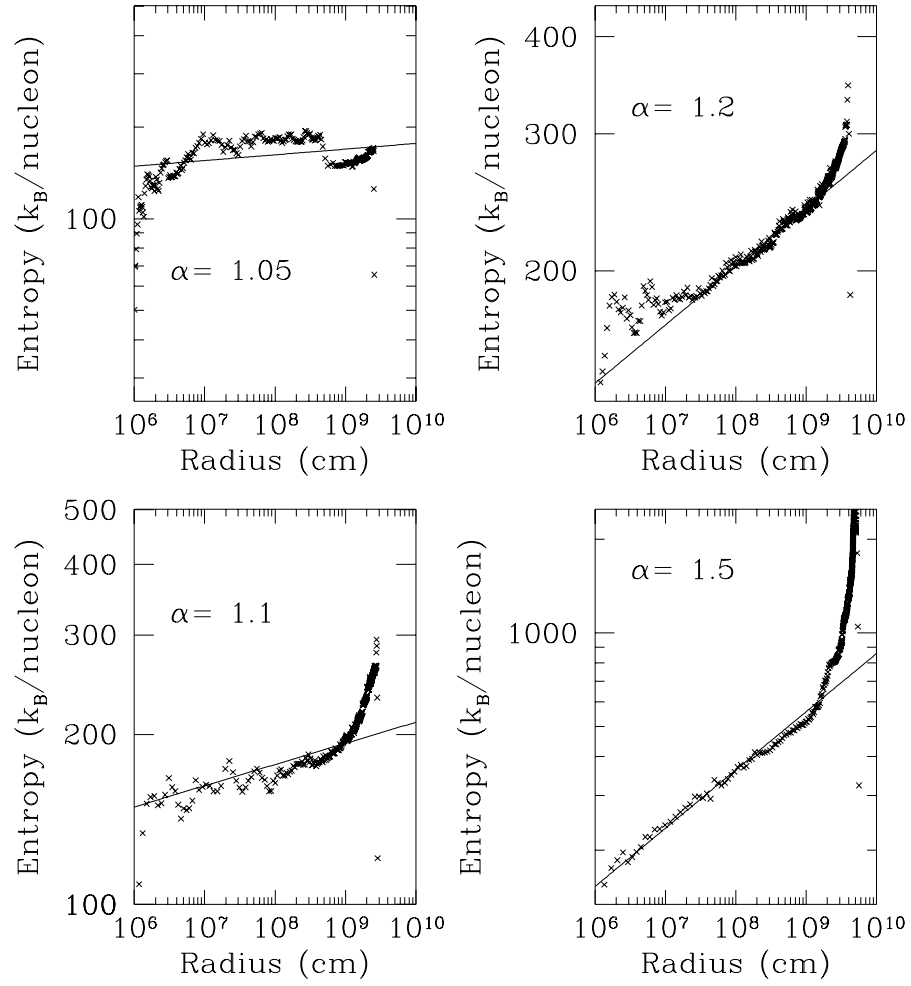


Fig. 3.— Entropy comparisons of simulations with analytic derivations for a range of α 's. Except at large radii where photons are no longer trapped, the analytic model matches the simulations for all values of $\alpha > 1$.

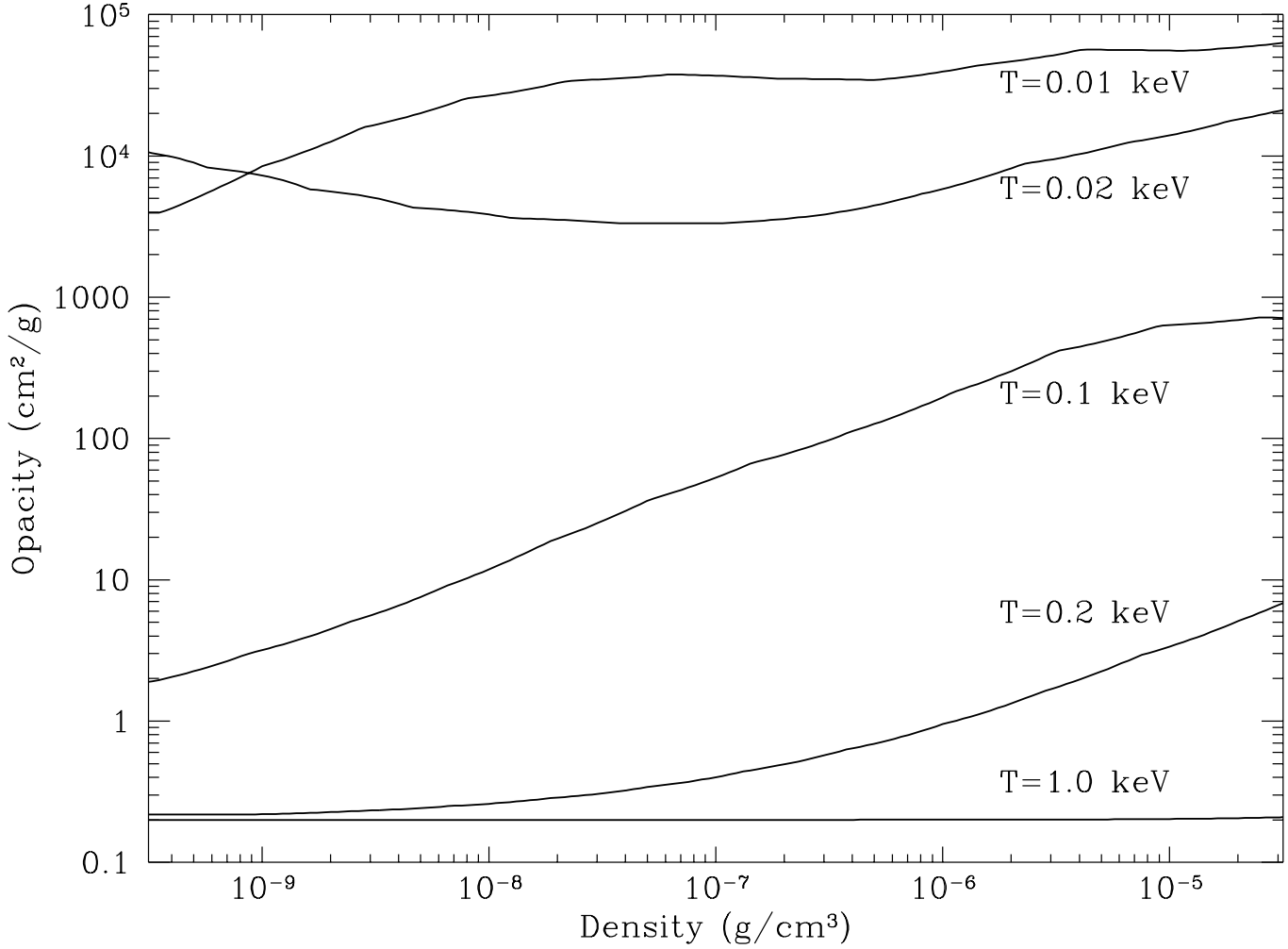


Fig. 4.— The iron opacity for a range of densities. The different lines are for different temperatures. Note that as the temperature drops from 0.2 keV to 0.1 keV, the opacity increases by ~ 2.5 magnitudes. This jump creates the sharp transition from the roughly electron-scattering opacity regime to the regime dominated by recombined iron.

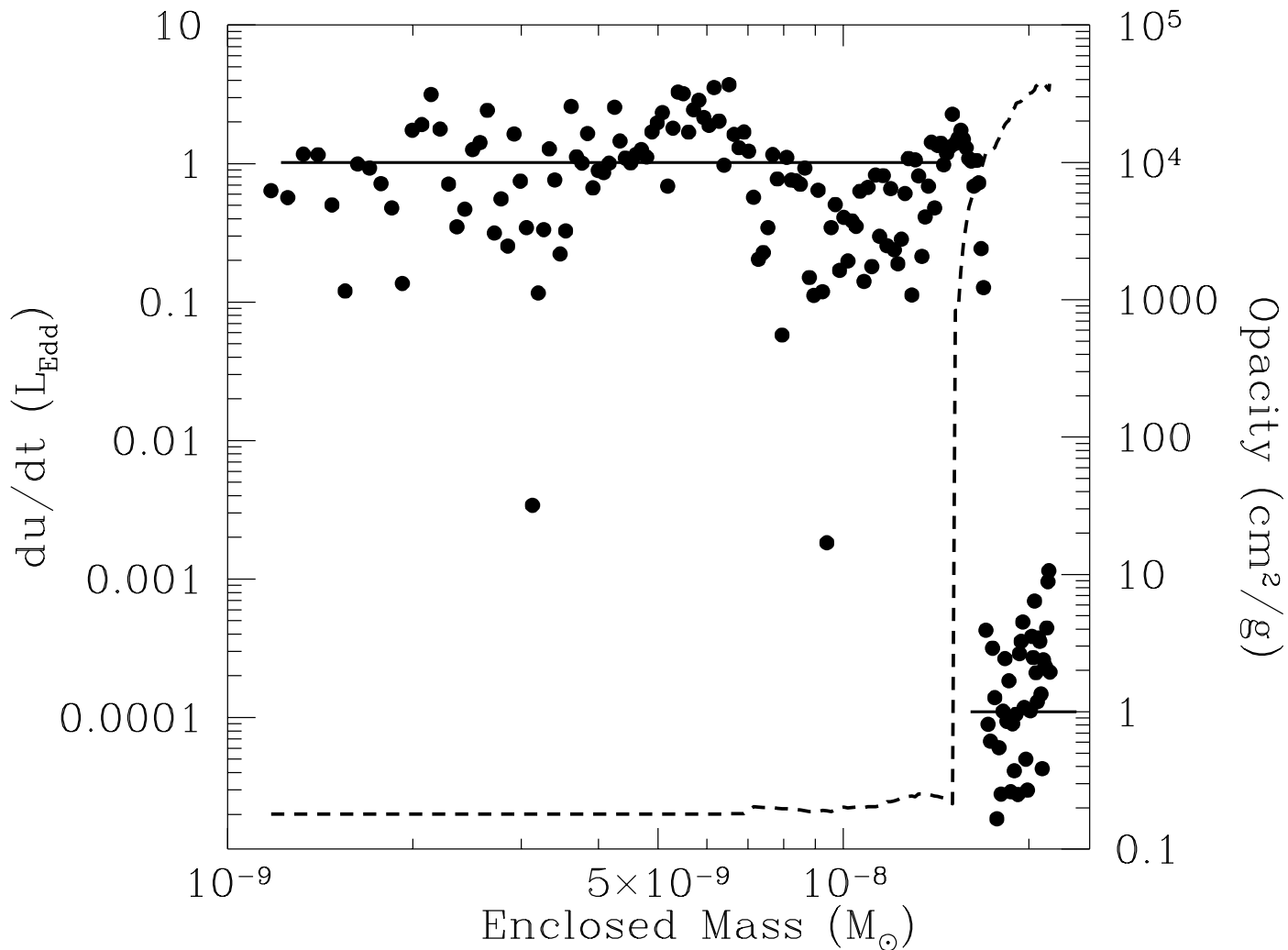


Fig. 5.— Luminosity (dots and solid line) and opacity (dotted line) vs. radius in the neutron star atmosphere. The dots mark each cell in the simulation. (The scatter exists because the diffusion is not in strict equilibrium and the diffusion varies slightly each time step). The net effect is that the inner atmosphere, whose opacity source is electron scattering has a luminosity roughly equal to the Eddington Luminosity. When the opacity increases dramatically due to recombined iron, the luminosity drops to roughly $10^{-4}L_{\text{Edd}}$. It is this luminosity that we observe. This very large difference in luminosity is the energy supplied to the binding energy of the wind. The sharp transition in opacity is due to the sensitivity of the opacity on the temperature (see Figure 4).

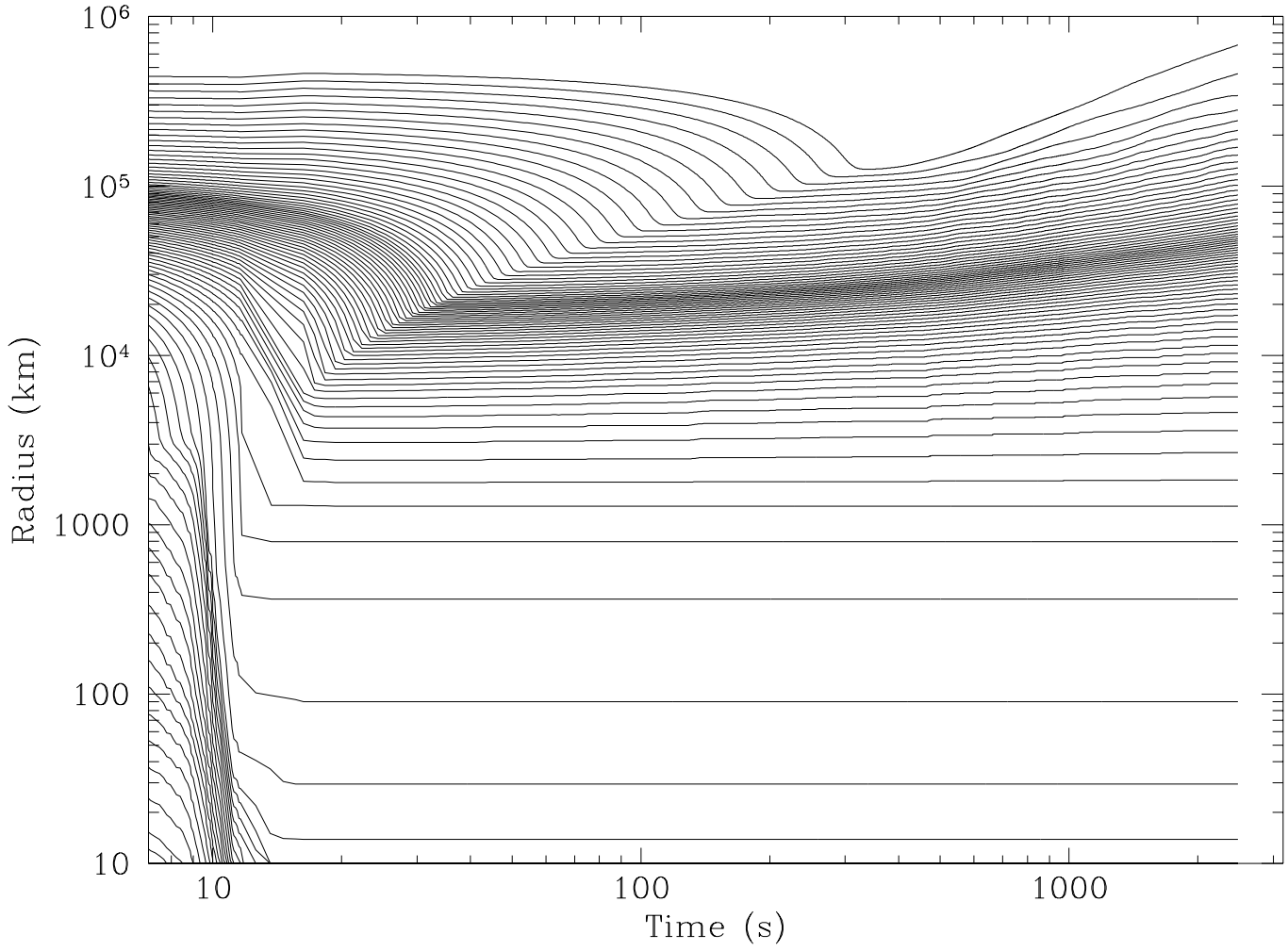


Fig. 6.— Mass-trajectory plot. Note that the initial material is accreted rapidly as it compresses due to neutrino cooling and exceeds the critical density. At late times, photon cooling drives a wind and the outer atmosphere expands.

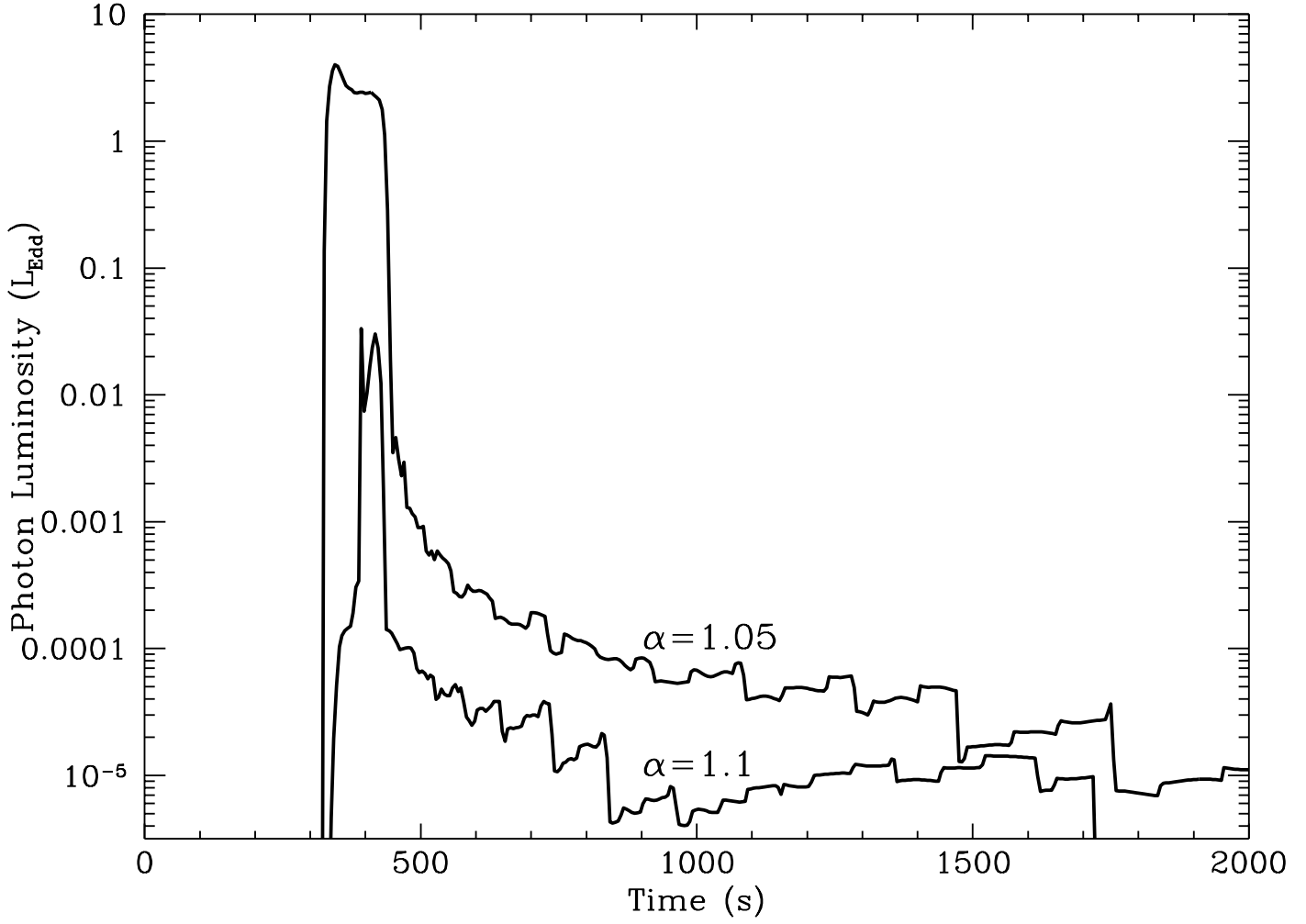


Fig. 7.— Luminosity of the accreting neutron star system vs. time. Note that the luminosity quickly drops to roughly $10^{-4}L_{\text{Edd}}$ and remains low for the duration of the simulation. During this time, the outer atmosphere blows off in a photon-driven wind.

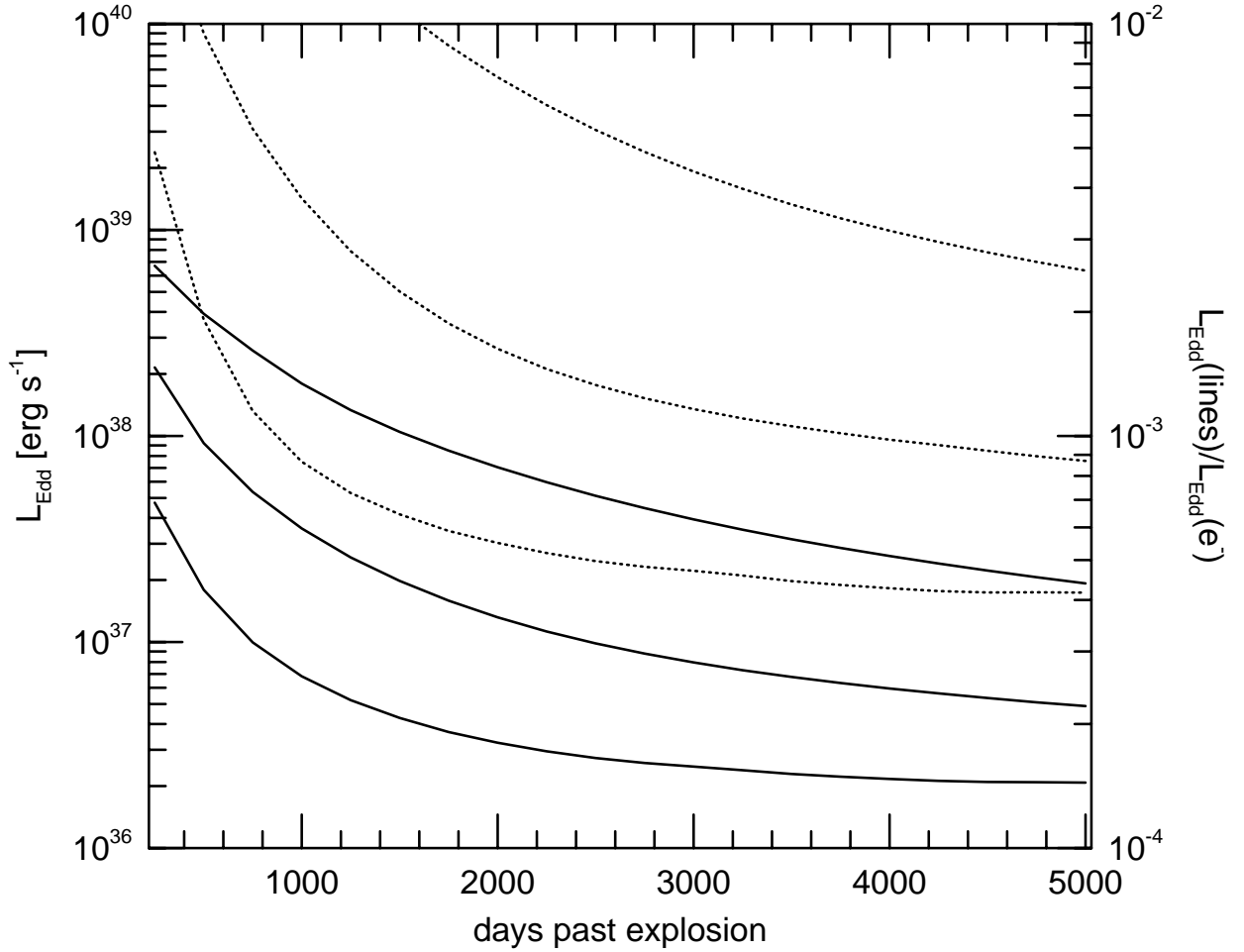


Fig. 8.— Eddington limit including the effect of lines in a plasma composed of Fe, Co, and Ni in solar ratios and with a density of 10^{-8} (lowest curve), 10^{-7} , and 10^{-6} g cm^{-3} in homologous expansion. The solid lines show the Eddington luminosity. The dotted lines show the factor by which the electron-scattering Eddington limit is multiplied by the addition of line opacity.